Research Article Vol. 58, No. 16 / 1 June 2019 / Applied Optics 4337

applied optics

Vignetting correction for a single star-sky observation image

Di Zhang,[1,2,3] Qing Yun Yang,[1,*] and Tao Chen[1]

[1]Changchun Institute of Optics, Fine Mechanics and Physics, Chinese Academy of Science, Changchun 130033, China
[2]University of Chinese Academy of Sciences, Beijing 100049, China
[3]e-mail: ilhatu@163.com
*Corresponding author: yangqingyun@ciomp.ac.cn

Received 4 February 2019; revised 30 April 2019; accepted 1 May 2019; posted 1 May 2019 (Doc. ID 359435); published 24 May 2019

We propose a method for robustly determining the vignetting function given only a single star-sky image taken by a large-aperture optical system. The actual large-aperture optical system is complex and difficult to model. Thus, the proposed method is designed to determine vignetting distortion of star-sky images without knowing the parameters or model of the optical system. This method is a model-free method by applying a polynomial regular term to the expectation-maximization algorithm to correct vignetting distortion. Unlike prior approaches to single-image vignetting correction, our proposed method, which does not rely on the optical model, gives more accurate results. The effectiveness of this technique was verified using real star-sky images captured with a large-aperture optical system (2-m telescope).

https://doi.org/10.1364/AO.58.004337

1. INTRODUCTION

The vignetting effect refers to a position-dependent loss of light in the output of an optical system. This occurs mainly due to the effective size of the aperture stop, which blocks part of the incident ray bundle thereby resulting in gradual fading of an image at points near the periphery [1]. Several factors contribute to vignetting. Some arise from the optical properties of camera lenses, the most prominent of which is off-axis illumination falloff or the cos4 law [2].

Vignetting distortion of an optical system is a significant problem for a ground-based large aperture telescope. It not only reduces the image signal-to-noise ratio (SNR) and image quality but also makes it so the dim targets of the edge cannot be detected. It also influences applications that rely on the accuracy and intensity uniformity of the scenes, such as star-sky image splicing, matching, segmentation, optical flow estimation, and dim space-target extraction and tracking. For these applications, the correction of the vignetting effect is an important preprocessing step in achieving high-quality results.

At present, the main methods of vignetting correction with one star-sky image can be divided into flat-field [3] and model-based methods [4–13]. The flat-field method usually takes an image in a uniform scene region and measures the corresponding intensity response at each pixel position. In such response images, variations in brightness directly reflect the transfer function of the vignetting effect [4–8]. This method is simple to understand and may seem easy to apply for any optical system. On the other hand, Kang and Weiss estimated the vignetting function based on vignetting model information [8]. Some later model-based methods usually need to estimate the actual image center and vignetting function [11–13].

However, the vignetting correction methods presented above usually need the specific information of the optical system or vignetting model. In fact, in some cases vignetting should be corrected without any knowledge of the optical system parameters and model information. On one hand, the flat-field method requires that the brightness of the light source is absolute uniform, and the flat-field image can be available during the observation. However, it is difficult to obtain an absolute uniform light source. In general, we do not know the information of the flat-field, and we have only the original image, so the flat-field method is not applicable to this case. On the other hand, the model-based method cannot solve complex vignetting due to the complexity of an actual optical system, for it is difficult to model the vignetting function. Specifically, the off-center axis of the camera and the tilt of the camera can make vignetting asymmetrical and irregular. Besides, various unknown lens and aperture parameters also affect the shape of the vignetting function [14], making it impossible to model the vignetting function for an existing camera.

In this paper, to solve the problem of vignetting correction with a single star-sky image obtained from an unknown optical system, we propose a model-free method by applying a polynomial regular term to the expectation-maximization (EM) algorithm. The correction of single-image vignetting presents challenges, which mainly lie in differentiating global intensity variations caused by vignetting from other sources of intensity

variation. An actual star-sky image is composed of noise, background light, star points, and halo. The background light shows slow spatial variation, and it is reasonable to assume that background light is uniform in vignetting-free images. Variation in background brightness directly reflects the transfer function of the vignetting effect. Thus, we can estimate the vignetting function from the background light.

The remainder of this paper is organized as follows. Section 2 introduces several reasonable assumptions that play an important role in vignetting correction. Section 3 introduces our method, and provides the specific implementation procedure. Simulations and experiments are presented in Section 4. In Section 5, we conclude the paper.

2. ASSUMPTION INTRODUCTION

In this section, to realize the algorithm in this paper, the following two assumptions are added according to the actual situation. Based on these assumptions, we derive the process of calculating the formula.

As the basic assumption of the algorithm, the images obtained at an observatory have a uniform background, and the background directly reflects the vignetting effect. Under normal circumstances, an observatory should be built on higher ground, thereby benefiting from clear nights, lower atmospheric water vapor content, and high astronomical visibility. Scattering occurs when starlight is transmitted through the atmosphere, forming a dim uniform background in a small field of view. Background brightness directly reflects the transfer function of the vignetting effect; thus, we can solve the vignetting function through background brightness.

Another basic assumption of the algorithm is the smoothness of vignetting function. We need to determine the characteristics of the vignetting function prior to conducting image processing, since the beam from the off-axis point filled with the incident pupil is partially blocked by some optical components and cannot pass through the optical system completely. This occlusion process is continuous and the luminous flux varies continuously with the angle; thus, the vignetting function is also continuous and smooth.

According to previous models, the loss of light due to the vignetting function can be expressed as the following approximation [8] (see [16], p. 346):

$$I_{\mathrm{VIG}} \approx \frac{1}{\left(1+\left(\frac{r}{f}\right)^2\right)^2}\cdot(1-\alpha r)\cdot I_0, \qquad r\in[0,r_0]. \tag{1}$$

This provides a reasonable model for common digital cameras but is inconsistent with large-aperture astronomical telescopes. However, from this model, it also illustrates that the vignetting function is continuous and smooth. Therefore, the smoothness of images can act as an important assumption.

Based on the above two assumptions, a star-sky image I with vignetting can be described as follows:

$$I = V\cdot k + V\cdot T + \varepsilon, \tag{2}$$

where I consists of the low-frequency term $V\cdot k$ and the high-frequency term $V\cdot T+\varepsilon$. $V\cdot k$ is background light, V is the vignetting function, and k is the constant parameter that represents the vignetting brightness. $V\cdot T+\varepsilon$ represent noise, star points, and the associated halo. ε is Poisson noise, and T is star points and associated halo.

The process can be summarized as

$$R = \frac{I}{V} = k + T + \varepsilon', \tag{3}$$

where R is the vignetting-free image. It is presumed that V shows slow spatial variation, and it is reasonable that $\varepsilon\approx\varepsilon'$, ε' also display Poisson noise. Therefore, I/V is an appropriate approximation of R. Here, / is the de-vignetting process [12]. In this study, the core of the algorithm is used to estimate the vignetting function V, from which we can easily obtain a vignetting-free image R.

3. METHODS

In this section, we first present the algorithm description that introduces the component parts and structure of the algorithm in detail and then list the algorithm procedure.

A. Algorithm Description

Because of the complexity of an actual optical system, the exact model of the equipment may be unknown. This precludes using the maximized log-likelihood function [17] directly to calculate the vignetting function; thus, we employ the EM algorithm to solve the vignetting function. The EM algorithm is mainly divided into the estimation (E) step and the maximization (M) step of the EM algorithm.

The E step of the EM algorithm is to estimate the background. According to the assumption of local smoothness, the background of the image can be represented by a polynomial model. We use the Savitzky–Golay (SG) filter [15] to fit the image with local polynomial least squares. The M step of the EM algorithm is to update the image. Using statistical information on the difference image (original image minus SG fitting image), we divide the current image into the uncertain region (star points, noise, and halo) and the reliable region. Then, we replace those pixels in the uncertain region with the SG fitting value, and the data in the reliable region was retained.

We continue to update the background estimation based on the current image, iteratively updating the value of the pixels in the uncertain region. The iterative process continues until the termination conditions are satisfied. The result of the iterative process is the "background" we expect. According to the above assumptions, the background reflects the vignetting function. Since there is still some noise in the background, the vignetting function is the result of the "background" SG fitting and normalization. Then the vignetting-free image is recovered by de-vignetting process.

An important step in each iteration is the estimation of the background. Traditional low-pass filtering algorithms include linear and nonlinear filters, which tend to blur the images. Spatial averaging of images is one of the simplest filtering methods applied to vignetting correction [18]. However, pixels in images with high brightness and high frequency usually have a significant influence on the filtering result. Here, we employ the SG filter to estimate the background. The effect of the SG filter varies with the selected window width. It can be easily used to keep a specific low-frequency component. Besides,

it can satisfy the local smoothness of the background. Thus, we use it to estimate vignetting function V from image I.

Another important step in each iteration is to distinguish the uncertain region (star points, halo, and noise). The difference-image between the star-sky image and the filtered image is generally approximated as a single Gaussian distribution in engineering.

Therefore, the single Gaussian background model method is used to distinguish the background from the target, and the threshold is set as $2\delta \sim 3\delta$ according to practical experience. If bright stars are surrounded by a faint halo caused by scattering and charge-coupled device (CCD) blooming noise, it is a challenge to distinguish the background and halo owing to lack of textural information. Therefore, the classification threshold should be decreased, thereby reclassifying a proportion of the background pixels as belonging to the uncertain region awaiting processing.

B. Algorithm Procedure

The algorithm flow is shown in Fig. 1.

The algorithm presented in this paper can be summarized as follows:

Step 1: Estimate the background. The SG filter is used to estimate the background:

$$E_k = f_{SG}(I, W), \tag{4}$$

where $f_{SG}(,)$ is a three-order SG filter, and E_k is the estimation of the background image for the kth iteration. I is the input image, and W is the width of the filter window.

Step 2: Update the image and the uncertain region. First, we calculate the difference image of kth iteration, D_k:

$$D_k = I - E_k. \tag{5}$$

Then, we calculate standard deviation δ of D_k. We set a threshold to distinguish the uncertain region:

$$\Delta \in (2\delta, 3\delta). \tag{6}$$

We also set limits on the number of uncertain regions:

$$\mathrm{sum}(S) \le \alpha \cdot \mathrm{length}(I) \cdot \mathrm{width}(I). \tag{7}$$

Here, α is the threshold for the proportion of the uncertain region within the image (set to 50%), above which extension of the uncertain regions is terminated. Equations (8) and (9) are as follows:

$$S_k = \begin{cases} S_k(i,j) = 1, & |D(i,j)| \ge \Delta \quad \text{and} \quad \mathrm{sum}(S_k) < \alpha \\ S_k(i,j) = 0, & |D(i,j)| < \Delta \quad \text{and} \quad \mathrm{sum}(S_k) < \alpha \end{cases}, \tag{8}$$

$$S_k = S_{k-1}, \qquad \text{if } \mathrm{sum}(S_k) < \alpha. \tag{9}$$

Here, S_k is the record matrix of the uncertain region for the kth iteration; if the difference image is $\ge\Delta$, we set the corresponding position of record matrix $S_k(i,j) = 1$. In Eq. (10),

$$S = \mathrm{sgn}\left(\sum_{1}^{k} S_k\right), \tag{10}$$

where S is the record matrix of the uncertain region, and S is the union of S_k from the 1th iteration to the kth iteration. For Eq. (11),

$$I(i,j) = \begin{cases} E(i,j), & S_k(i,j) = 1 \\ I(i,j), & S_k(i,j) = 0 \end{cases}, \tag{11}$$

such than if pixel $I(i,j)$ belongs to the uncertain region, we replace it with $E(i,j)$. Finally, we update image I in each iteration.

Step 3: Determine whether any termination condition is satisfied. If true, go to Step 4; otherwise, go to Step 1.

Convergence termination condition is as follows:

$$\frac{\delta_k - \delta_{k-1}}{\delta_k} \langle \varepsilon \text{ and } k \rangle 1. \tag{12}$$

Here, ε is the threshold of convergence. In this paper, we use the standard deviation of the difference image of the kth

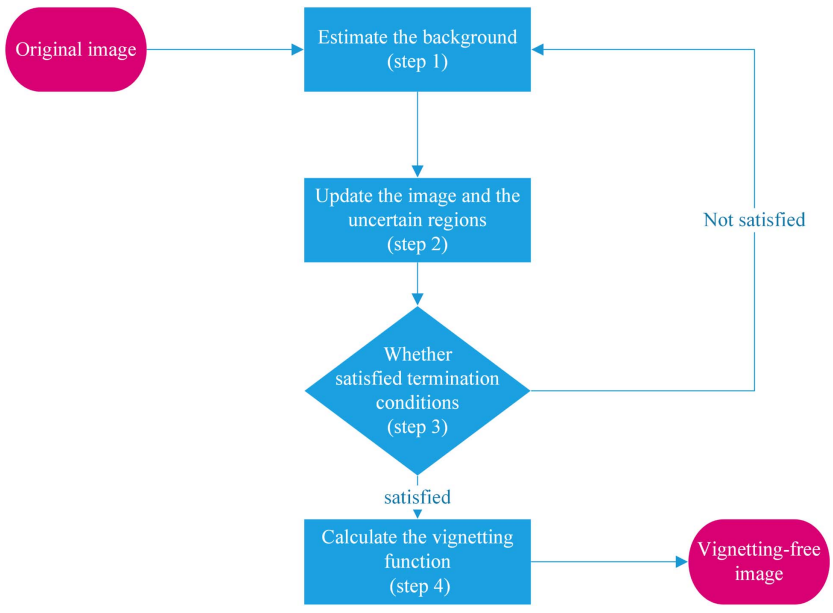

Fig. 1. Flow chart of our algorithm.

iteration δ_k to describe convergence. The termination condition is satisfied when the error of the standard deviation is less than ε. This condition indicates that the iterative process is terminated when the standard deviation converges.
Step 4: Calculate the vignetting function:

$$V = \frac{E_{k+1}}{\max(E_k)}. \tag{13}$$

We obtain the vignetting function V through the normalized background E_{k+1}. In Eq. (14),

$$R = \frac{I_0}{V}. \tag{14}$$

Finally, the vignetting-free image is equal to the original image I_0 divided by the vignetting function V.

4. SIMULATIONS AND EXPERIMENTS

In this section, to verify the effectiveness and practicability of the algorithm in this paper, we carry out experiments on this algorithm. We first carried out the experiments with the synthetic vignetted image data set in Section 4.A and analyzed the experimental results. Then, we carried out the experiments with the real vignetted image data set in Section 4.B and show the images before and after processing. Both of above two experimental results on image data sets (in the visible band with a 2-m aperture telescope) all demonstrate the effectiveness of our method. Finally, the parameters' setting of our algorithm is discussed.

A. Simulations

We generated a synthetic image to evaluate the performance of the proposed method. The simulated vignetting effect was generated according to the model [8]. We synthesized the vignetting function and applied the synthesized vignetting function to the test images. This derives ground-truth images for both the vignetting functions and the synthetic images, thereby enabling quantitative evaluation of the performance of the proposed method. We applied our method to the image, as illustrated in Fig. 2.

The performance evaluation was carried out in such a manner that the similarity between the corrected image and the ground-truth image was calculated. For this purpose, we introduce the root mean square error (RMSE) to evaluate the accuracy of the vignetting function and image correction. A smaller RMSE indicates that the ground-truth image and corrected image errors are small; i.e., the estimation is more accurate. We evaluate the performance of the proposed method by comparing

Table 1. Result of Above Synthetic Vignetted Image Restoration[a]

Method	MSE	PSNR
Vignetting function	6.51×10^{-8}	64.27
Synthetic vignetted image	5.18×10^{-10}	84.13

[a]The RMSE and peak SNR of the vignetting function and image are shown, respectively.

Table 2. Comparison of Average Execution Time

Image-size	PC (GHz)	Running-Time (s)	Method
450×600	2.39	29	Zheng
450×600	2.10	0.7	Ours
$2k \times 2k$	2.10	9.29	Ours

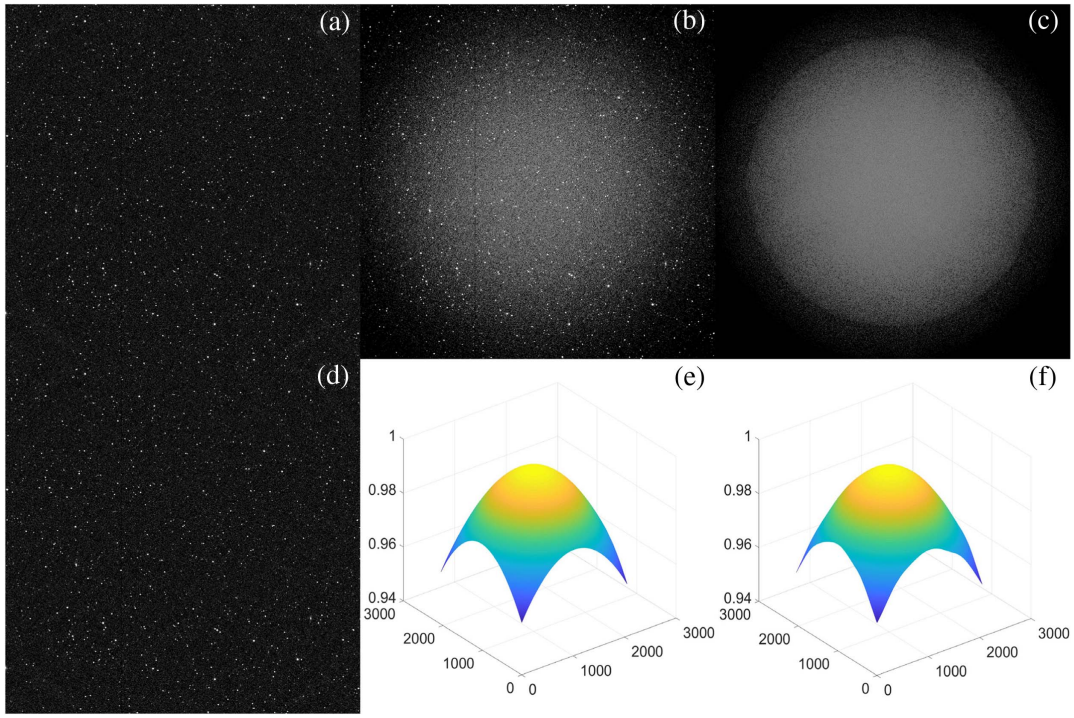

Fig. 2. Examples of restoring synthetic vignetted images: (a) ground-truth image with no obvious vignetting effect; (b) synthetic vignetted image; (c) background image (d) corrected image of synthetic vignetted image; (e) original vignetting image; (f) estimation of vignetting image.

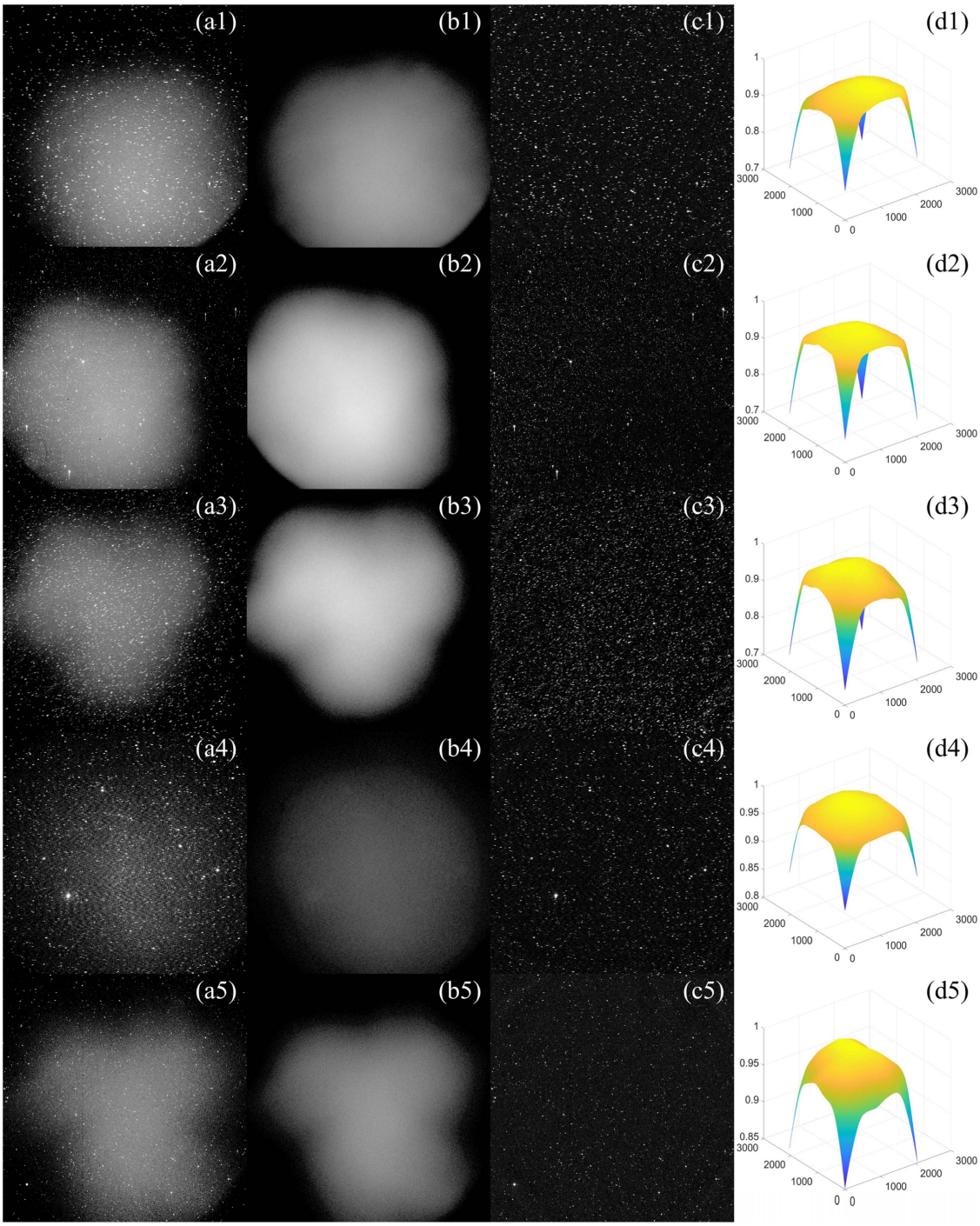

Fig. 3. Experimental images of star-sky images: (a1)–(a5) the original images; (b1)–(b5) the background images; (c1)–(c5) the corrected images; (d1)–(d5) vignetting images.

it to Zheng's original method [11]. The results in Table 1 show that the proposed algorithm has a good correction effect for the synthetic vignetted images, resulting in very accurate images.

As Table 1 shows, the accuracy of our method is better than that of Zheng *et al.* [11]. Our method has a high accuracy.

We also compare the speed of our method to that of the previous single-image vignetting correction method [11]. The algorithm presented in this paper is applied to a set of 70 sample star-sky images. Our algorithm is implemented in nonoptimized MATLAB R2017a and executes on a DELL PC (2.10 GHz Intel Xeon CPU E5-2620 v4). On average, our algorithm achieves speedups of 30–40 times that of Zheng *et al.*'s algorithm (see Table 2). A substantial increase in speed is likely to be possible with an optimized C++ implementation.

Because our algorithm does not rely on a vignetting model to estimate the vignetting function, it is applicable to the vignetting function of any parameter. More complex vignetting functions are difficult to simulate in this experiment, and even

more difficult to model. Therefore, it could not be verified experimentally, only by means of real vignetted images.

B. Experiments

The results of testing using the proposed method on real vignetted images are presented. In contrast to the results in Section 4.A, because we cannot have a proper reference image without knowing the vignetting function for real images, we only show the experimental results after vignetting correction. As we described in Section 4.A, however, the effectiveness of the proposed methods against real images may be anticipated from the results of synthetic images. In particular, the improvement of image quality, which can be visually identified from Figs. 3 and 4, verifies the effectiveness shown in Section 4.A.

In Fig. 3, (a1)–(a5) show the original images, which are input images to the algorithm; (b1)–(b5) are the background images resulting from the background estimation. Following normalization, we obtain the vignetting functions (d1)–(d5); (c1)–(c5) are the corrected vignetting-free images that are output from the algorithm; the grayscale of images in Fig. 3 is stretched such that the details can be easily displayed.

A detailed description of the changes and convergence in the image during the iterations can be seen in Fig. 5.

As these results show, following correction, the restored image does not display an obvious vignetting effect. The estimation of the vignetting function is shown in Figs. 3(c1)–3(c5). We also show the corrected image and original image in the scanlines in Fig. 4. It should be pointed out that the real vignetting function of a large-aperture optical system may not match the general Kang–Weiss model, for example in the case of an octagonal aperture. Furthermore, in practice, large-scale optical systems are complex, and there may be some differences between systems. Compared to model-based methods, our method is better suited to resolving complex vignetting. The experimental results in

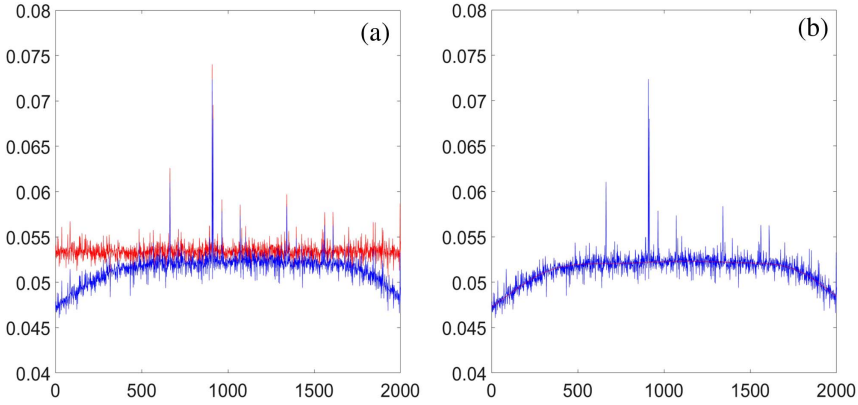

Fig. 4. (a) Distribution of corrected image and original image in the scanline. (b) The distribution of vignetting function and original image in the scanline.

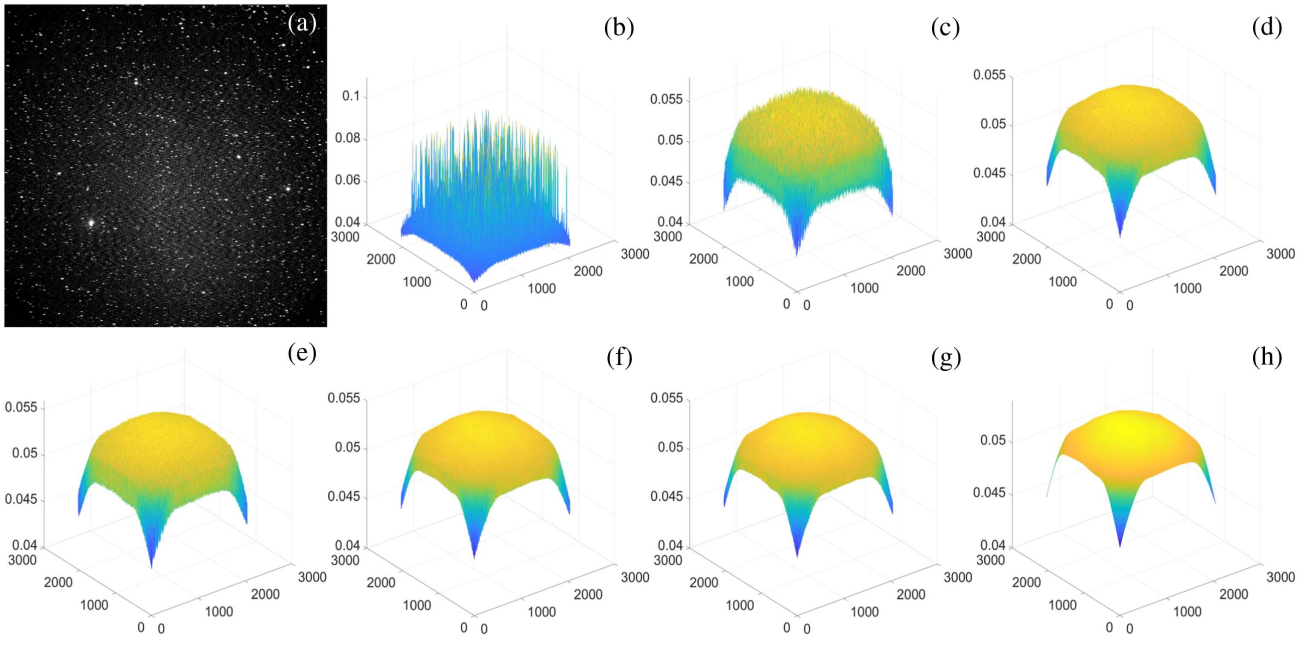

Fig. 5. (a) Original image; (b)–(g) images I in each iteration from the first to 7th iteration; (h) the background image after smoothing.

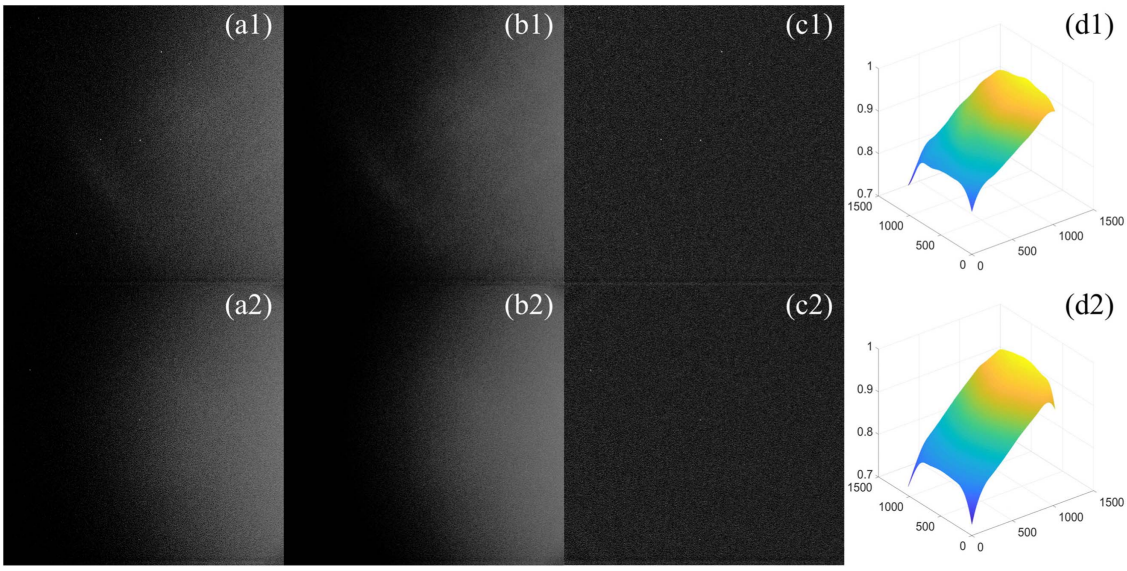

Fig. 6. Those images are the correction process of vignetting and stray light. (a1), (a2) the original images; (b1), (b2) the background images; (c1), (c2) the corrected images. (d1), (d2) the vignetting function.

Fig. 3 show that the effect of complex vignetting can be significantly removed.

C. Other Discussion

The successful application of the proposed method heavily depends on proper acquisition of images. Although we capture images on a clear night, the only limitation to the proposed method is that we should avoid stray light when capturing images.

Stray light also conforms to the local smoothness. If there is a moonlight halo or uneven atmospheric scattering, resulting in an image with both stray light and vignetting, this method in this paper can still correct the images and suppress the influence of stray light on the image uniformity (for example, in Fig. 6).

D. Parameters' Setting of Algorithm

The settings of the main parameters will be discussed in this section, including the termination condition of the iterative algorithm ε, the size of the filter template W, the orders of the filter, and the distinguishing threshold of uncertain region Δ.

The EM algorithm needs a termination mechanism; it cannot iterate indefinitely. We set a very small constant ε (0.01) to determine whether to stop. When $\frac{\delta_k - \delta_{k-1}}{\delta_k} < \varepsilon$, it indicates that pixels vary a little in each iteration and that the iteration should be stopped.

The order of the filter directly affects the filtering result; too small will lead to blurring, and too large will lead to overfitting. The third-order filter used can properly approach the vignetting function well without blurring and overfitting, and is well applied to the algorithm.

As for the choice of the filter template size W, our algorithm is robust and insensitive to the selection of the template length. But it should not be too small. W and Δ can be appropriately adjusted for different image sizes and field angles in other data sources. Generally, the size of the filter template is 3–5 times the size of star points to eliminate the interference of star points and Δ at least larger than 2δ. In this paper, we use the size of the filter template from 64 to 128, but the results are the same.

To ensure that the information of the image is always fully utilized, the proportion of the threshold of the uncertain region to that of the image, α was set to 50%.

5. CONCLUSIONS

This paper proposed a method for determining an image vignetting function given only a single star-sky image taken from the large-aperture optical system. This method is a model-free method by applying a polynomial regular term to the EM algorithm to correct vignetting distortion. It can adapt to complex environments and extract vignetting information from a single image. This method has the advantages of a simple principle, highly accurate correction, fast convergence speed, and capability of dealing with the heterogeneity of a complex sky background, thus showing strong practicability.

The star-sky images' data set used in the experiments proved the efficacy of the proposed method. The method improves the image quality significantly under the conditions of complex vignetting and a complex skylight background. This method is applied not only to the condition that only vignetting exists but also to the condition that stray light and vignetting coupling exists. It is applicable to astronomical observation and remote sensing images, and has significant value for these applications. It can be applied to agricultural observation, ocean observation, and ground observation. This robust algorithm can also be used in medical detection and analysis and for high dynamic range imaging.

6. DISCUSSION

This method in is applicable to the large-aperture optical system in which the incident light varies continuously when observing the sky-star image. The proposed method is also

applicable to some other situations that require smooth background estimation or stray light suppression. For example, some moonlight and stray light evenly scattered from the sun behind the earth also can be suppressed.

We estimate the vignetting function from the background; the available background information should more than α. In a few cases, such as bright stars and halos that fill the whole image, the accuracy of the results cannot be guaranteed.

REFERENCES

1. E. Hecht, *Optics*, 4th ed. (Addison-Wesley, 2001), pp. 172–173.
2. M. Klein and T. Furtak, *Optics* (Wiley, 1986).
3. J. Manfroid, "On CCD standard stars and flat-field calibration," Astron. Astrophys. Suppl. **118**, 391–395 (1996).
4. N. Asada, A. Amano, and M. Baba, "Photometric calibration of zoom lens systems," in *International Conference on Pattern Recognition* (1996), Vol. **1**, pp. 186–190.
5. A. A. Sawchuk, "Real-time correction of intensity nonlinearities in imaging systems," IEEE Trans. Comput. **C-26**, 34–39 (1977).
6. W. Yu, "Practical anti-vignetting methods for digital cameras," IEEE Trans. Consumer Electron. **50**, 975–983 (2004).
7. W. Yu, Y. Chung, and J. Soh, "Vingetting distortion correction method for high quality digital imaging," in *International Conference on Pattern Recognition IEEE Computer Society* (2004).
8. S. Kang and R. Weiss, "Can we calibrate a camera using an image of a flat textureless Lambertian surface?" in *European Conference on Computer Vision* (2000), Vol. **2**, pp. 640–653.
9. S. Kim and M. Pollefeys, "Robust radiometric calibration and vignetting correction," IEEE Trans. Pattern Anal. Mach. Intell. **30**, 562–576 (2008).
10. D. B. Goldman, "Vignette and exposure calibration and compensation," IEEE Trans. Pattern Anal. Mach. Intell. **32**, 2276–2288 (2010).
11. Y. Zheng, S. Lin, S. Kang, R. Xiao, J. C. Gee, and C. Kambhamettu, "Single-image vignetting correction from gradient distribution symmetries," IEEE Trans. Pattern Anal. Mach. Intell. **35**, 1480–1494 (2013).
12. Y. Zheng, C. Kambhamettu, and S. Lin, "Single-image optical center estimation from vignetting and tangential gradient symmetry," in *IEEE Conference on Computer Vision & Pattern Recognition* (2009).
13. S. Lyu, "Estimating vignetting function from a single image for image authentication," in *ACM Workshop on Multimedia and Security* (2010), pp. 3–12.
14. R. Kingslake and R. B. Johnson, *Lens Design Fundamentals*, 2nd ed. (SPIE, 1978).
15. A. Savitzky, "Smoothing and differentiation of data by simplified least squares procedures," Anal. Chem. **36**, 1627–1639 (1964).
16. J. Strong and R. A. Sawyer, "Concepts of classical optics," Phys. Today **11**(10), 42–46 (1958).
17. Y. Zheng, S. Lin, C. Kambhamettu, J. Yu, and S. Kang, "Single-image vignetting correction," IEEE Trans. Pattern Anal. Mach. Intell. **31**, 2243–2256 (2009).
18. C. M. Bastuscheck, "Correction of video camera response using digital techniques," Opt. Eng. **26**, 1257–1262 (1987).